Journal of the Korean Society of Oceanography
Vol. 38, No. 3, pp. 143 — 155 September 2003

Circulation in the Central South Sea of Korea in Spring 1999

JAE CHUL LEE[1]*, SANG-HO LEE[2], DAE HYUN KIM[1], YONG TAE SON[2], HENRY T. PERKINS[3], JEONG-CHANG KIM[1], AND IG CHAN PANG[4]

[1]*Korea Inter-university Institute of Ocean Science, Pukyong National University, Pusan 608-737, Korea*
[2]*Department of Oceanography, Kunsan National University, Kunsan 573-701, Korea*
[3]*U. S. Naval Research Laboratory, Stennis Space Center, MS 39529, USA*
[4]*Department of Oceanography, Cheju National University, Cheju 690-756, Korea*

Current and sea level were observed in spring 1999 by a bottom mounted ADCP and tide gauge in the central part of the South Sea of Korea. With respect to the front, the distribution of isotherms is prograde in the offshore region whereas that of isohalines is retrograde, especially in the coastal area. The combined effect results in shoaling of isopycnals at the front. This distribution corresponds to a westward coastal flow on the northern side of the front and the eastward Tsushima Warm Current (TWC) to the south, determined by vessel-mounted ADCP observations. The low-frequency current shows either alternating clockwise-counterclockwise rotation or else persistent eastward motion depending on the frontal motion. Fluctuations of wind, sea level and current are coherent at period of 3-4 days and show some characteristics of Ekman-like dynamics.

Key words: South Sea of Korea, Tsushima Warm Current, Front, Sea level, Coherence

INTRODUCTION

The South Sea of Korea extends from the Cheju Strait eastward into the Korea Strait. Yellow Sea Water (YSW) including the Changjiang River Diluted Water and a small fraction of the Tsushima Warm Current (TWC) enter the South Sea through the Cheju Strait. Additional TWC enters from the south, east of the Cheju Strait. These water masses move eastward and enter the East (Japan) Sea through the Korea Strait. The mixture of coastal water and YSW is generally cooler and fresher than TWC water in most seasons except summer.

A characteristic front develops between the YSW/coastal water and TWC water. Lee (1983) and Lee *et al.* (1984) studied the structure and meander motion of this front. Although the waters in the South Sea are known to flow eastward, Lee (1983) suggested that the direction of circulation in the coastal region would be westward. According to Lee *et al.* (1984), meander motion of the front was sensitive to wind, and the gentle bottom slope could be a favorable condition for the instability of frontal meanders. This front with its meander motion can be clearly seen in satellite infrared imagery (Ro *et al.*, 1995). There is no doubt that the variability of subtidal current is largely associated with frontal motion, which can be investigated by the long-term mooring of current meters.

Long-term current observations by moored instruments have been conducted in the Yellow Sea (Hsueh, 1988; Teague *et al.*, 1998), Cheju Strait (Chang *et al.*, 2000) and in the western channel of the Korea Strait (Shim *et al.*, 1984; Lee *et al.*, 1998). But, in the South Sea of Korea, there have been no such observations until 1999. In order to study the variability of the current and sea level, bottom-mounted ADCP, vessel-mounted ADCP (V/M ADCP) and CTD observations were carried out from March through May 1999 in the central part of the South Sea.

OBSERVATIONS

A TRBM (Trawl Resistant Bottom Mount) with a set of ADCP (RD Instruments, 150 kHz) and a tide gauge (Sea Bird SB26) were deployed at the bottom of Site-M (34°01′N, 127°39′E) for 79 days from 11 March through 28 May 1999 (Fig. 1). The water depth was 80 m and velocity data were obtained at 10–74 m with 4 m interval. Because the front occurs where the water depth is 70–90 m (Lee, 1983), both average

*Corresponding author: jaechul@pknu.ac.kr

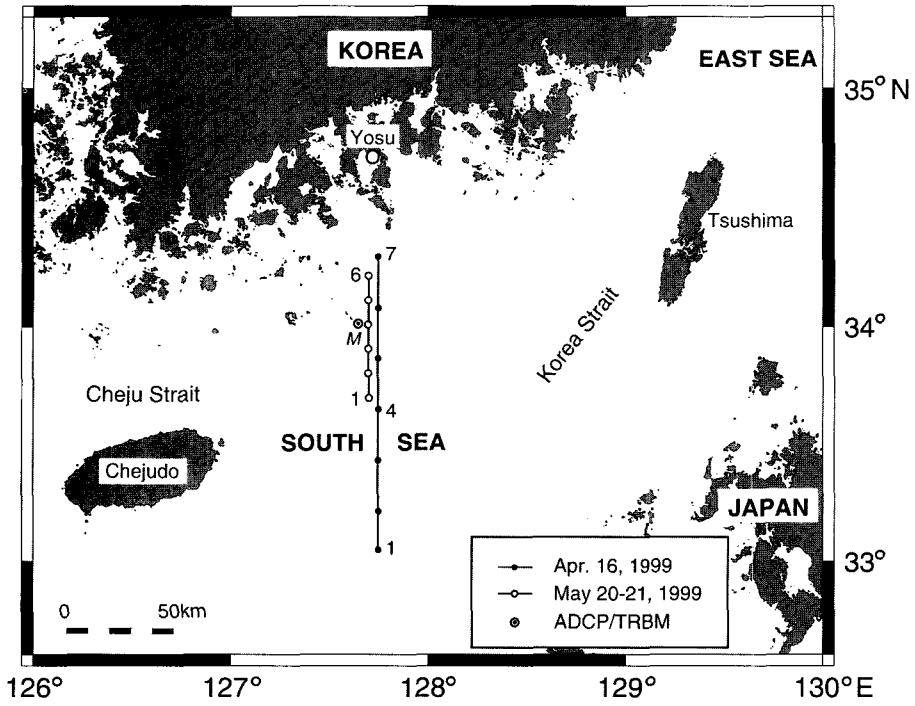

Fig. 1. Locations of ADCP deployment (Site-M) and CTD observations.

frontal position and movement of the coastal waters were considered in determining the mooring site. The CTD and V/M ADCP (RD Instruments, 150 kHz Narrow Band) observations were conducted by R/V *Tamyang* on 16 April and 20–21 May 1999 along the meridional sections shown in Fig. 1. In the latter cruise, V/M ADCP observations were repeated four times along the shorter section. Each section required three hours to complete and was repeated at six-hour intervals in order to reduce by averaging the influence of tides. CTD observations were also conducted three times, once between each pair of V/M ADCP sections. Hourly data of wind and sea level at Yosu were also used to compare with the current and sea level at Site-M, the ADCP/TRBM position.

HYDROGRAPHIC CONDITIONS

The ranges of temperature and salinity are 12–17 °C and 33.6–34.6 psu respectively in April, and are almost homogeneous in the vertical (Fig. 2). Temperature is about 13 °C at the latitude of Site-M, which is indicated by a black triangle on the upper scale of Fig. 2. Colder, fresher and denser water occupies the shallow coastal area. The horizontal change in salinity is small offshore from St. 5. Density is also nearly uniform vertically but the isopycnal of 25.6 becomes shallow near St. 5 then slopes down offshore. As will be shown in Fig. 7, St. 5 also coincides with a change in current direction, from weak westward flow near the coast to weak eastward flow seaward of that point. Therefore, St. 5 may be considered as the position of the front.

Fig. 3 shows the result of the CTD observations taken three times at six-hour intervals in May. Site-M has the same latitude as St. 4 in this shorter cross section. Compared with April, temperature has increased to 15–18°C but the salinity range has not changed. Although the general distribution of properties is similar in all three cases, the detailed isoline positions do vary. For example, the 17°C isotherm moves back and forth and the 34 psu isohaline has significant changes in shape and position. With increased surface heating and fresh water supply in May, stratification is stronger than in April. The thermal front has become prograde offshore of St. 4; that is, the isotherms deepen with increasing water depth. In contrast, isohalines are retrograde throughout most of the sections. The density section reflects both influences.The ADCP site (St. 4) is close to the center of shoaling isopycnals, away from which the current can have opposite directions, i.e., westward motion to the north and eastward motion to the south of this site. Because the Site-M is close to St. 4, the change in velocity measured by the bottom ADCP is sensitive to movement of the front.

Fig. 4 shows low-passed bottom temperature recorded by the ADCP. There is a seasonal trend of temperature

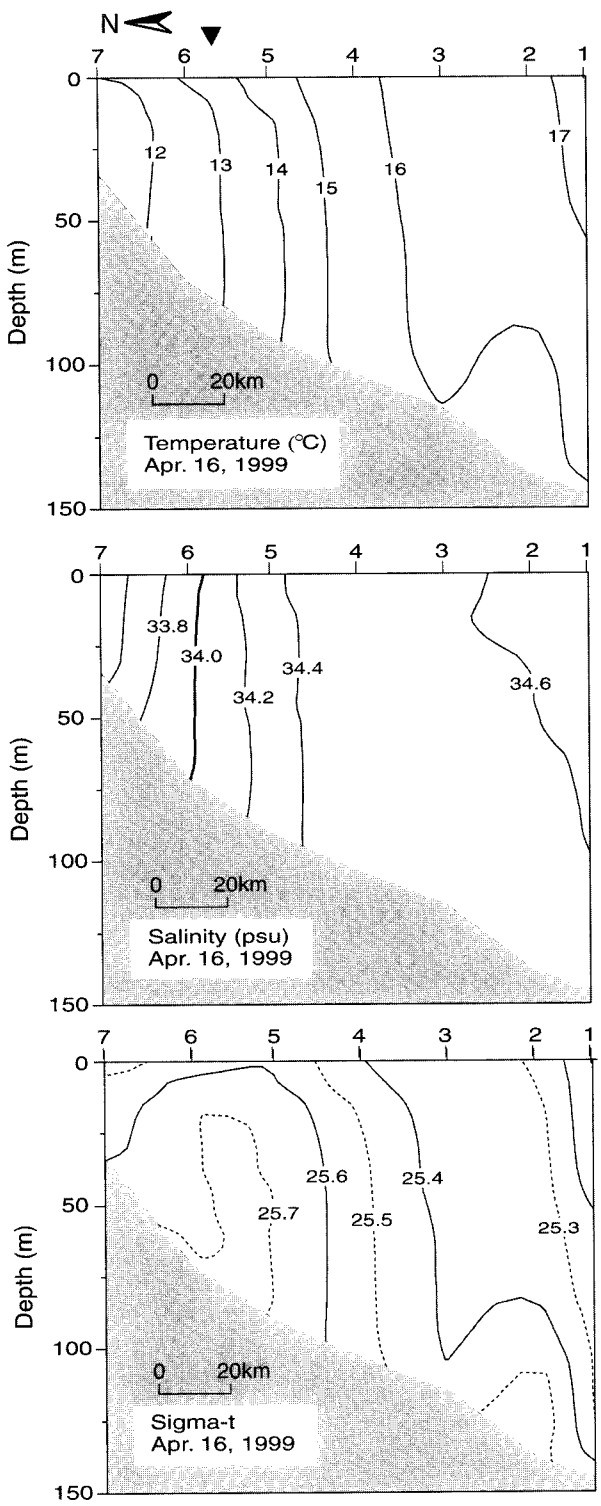

Fig. 2. Cross sections of temperature, salinity and density in April 1999. A dark triangle on the top denotes the position of Site-M.

increase from about 12.5°C in March to 15.5°C in May. At Site-M, horizontal temperature gradients on the bottom are greater in March-April than in May (Figs. 2 and 3), although vertical stratification is greater at the later time. It seems clear that the greater low-frequency temperature variability observed during March-April (Fig. 4) is due to the stronger horizontal temperature gradient at that time combined with lateral movement of the front in north-south direction, and that the reduced variability in May is associated with the weaker horizontal temperature gradient.

VERTICAL DISTRIBUTION OF VELOCITY

Sections with the vessel-mounted ADCP (V/M ADCP) were made before and after each CTD observation (Fig. 3), a total of four sections at six-hour intervals. Fig. 5 shows the E-component of velocity normal to the cross section. Eastward (positive) velocity is dominant in sections 1, 2, and 4, while section 3 has westward velocity of comparable strength. Because tidal currents are fairly large in the South Sea, the velocity fields in Fig. 5 must be processed for tide removal. If tidal inequality could be ignored, any two successive cross sections could be averaged to extract the approximate nontidal velocity. Although the time interval of six hours is often taken as suitable for averaging, actual conditions of tidal current will now be examined using the mooring data.

Hourly time-series of near-surface tidal velocity and sea level obtained from the harmonic analyses of ADCP/TRBM data are displayed in Fig. 6 during the V/M ADCP profiling. Vertical shaded bars on the graph indicate profiling times. Observation was carried out during successive high and low waters, but the inequality of tidal velocity is not small enough to be neglected. Without this information, separate estimates would be made by averaging the section pairs 1–2, 2–3, and 3–4 to get three sets of nontidal velocity. Fig. 6 suggests that only one such average velocity can be obtained from sections 2–3, because both flood and ebb velocities have nearly the same magnitudes. Hence, tidal contributions to the V/M ADCP data will largely cancel when averaged over those two intervals. The result of such averaging is illustrated in Fig. 7. Current is westward in the coastal region shallower than 70 m and has a maximum velocity of about 15 cm/s. The direction of current is reversed near St. 4 and velocity increases offshore to about 30 cm/s. As noted in the density fields of Fig. 3, the isopycnals slope oppositely from St. 3 or St. 4 to both sides, coinciding with the boundary where the current changes sign. This result supports the suggestion by Lee (1983) that the coastal circulation is toward the west.

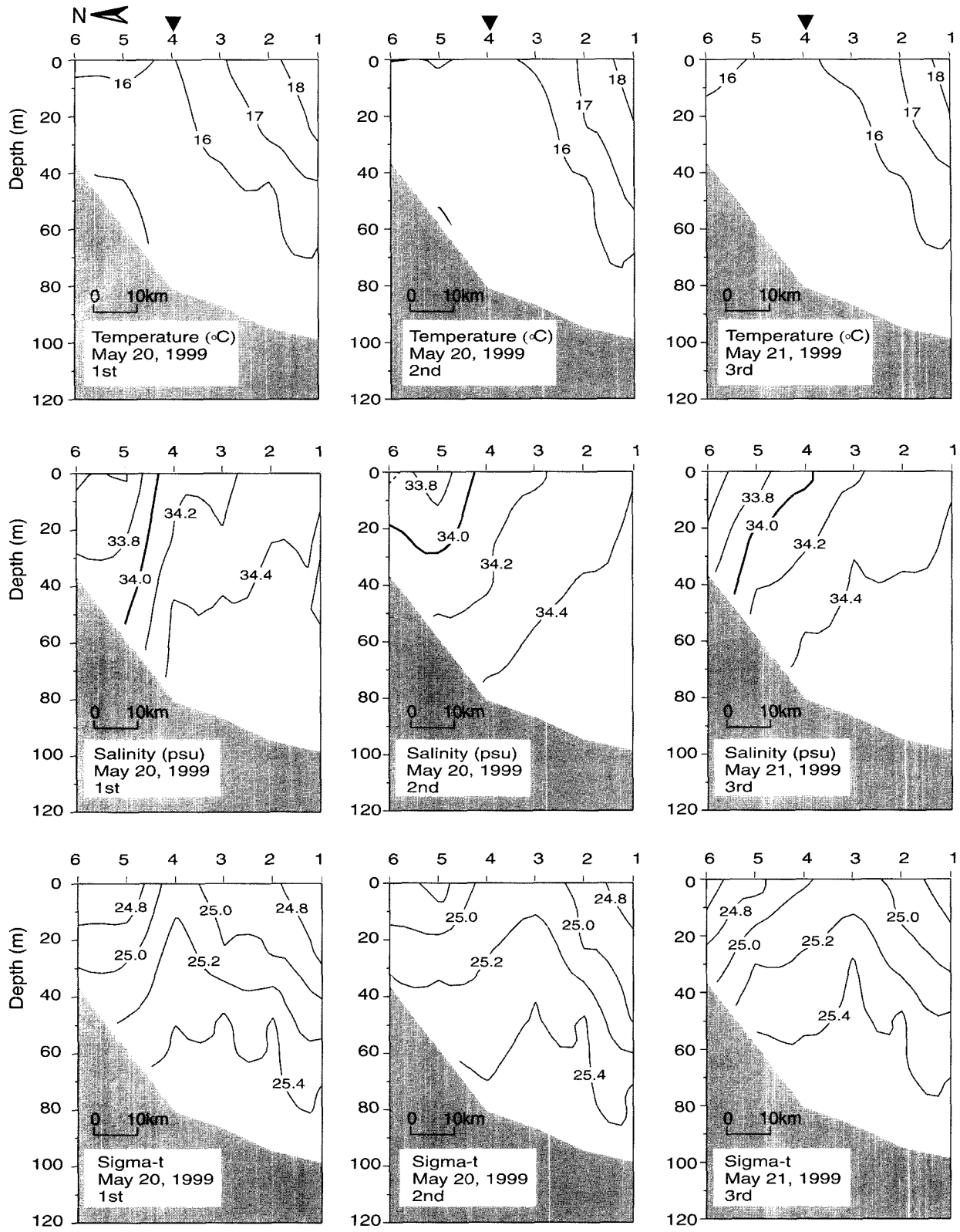

Fig. 3. Same as Fig. 2 except in May 1999.

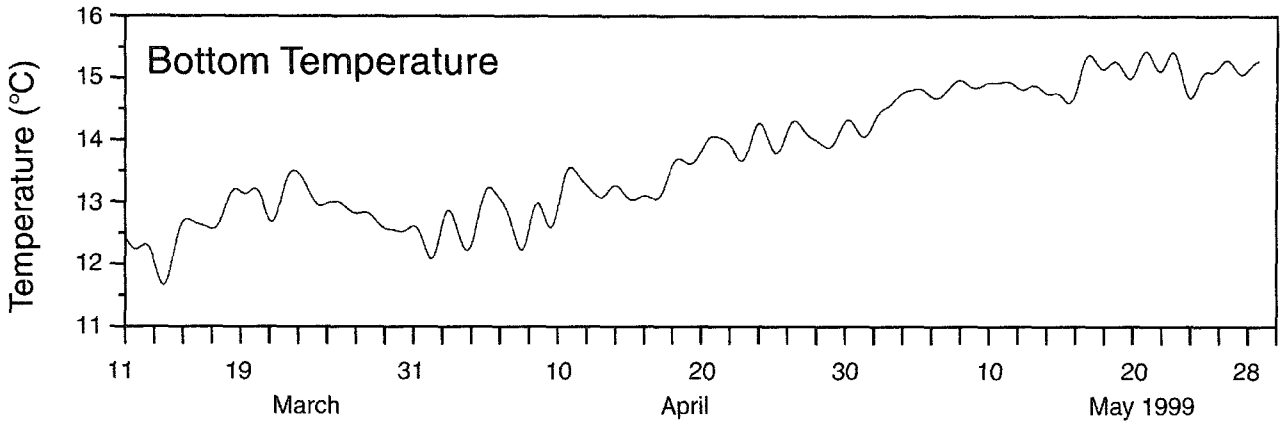

Fig. 4. Time series of low-passed bottom temperature at Site-M.

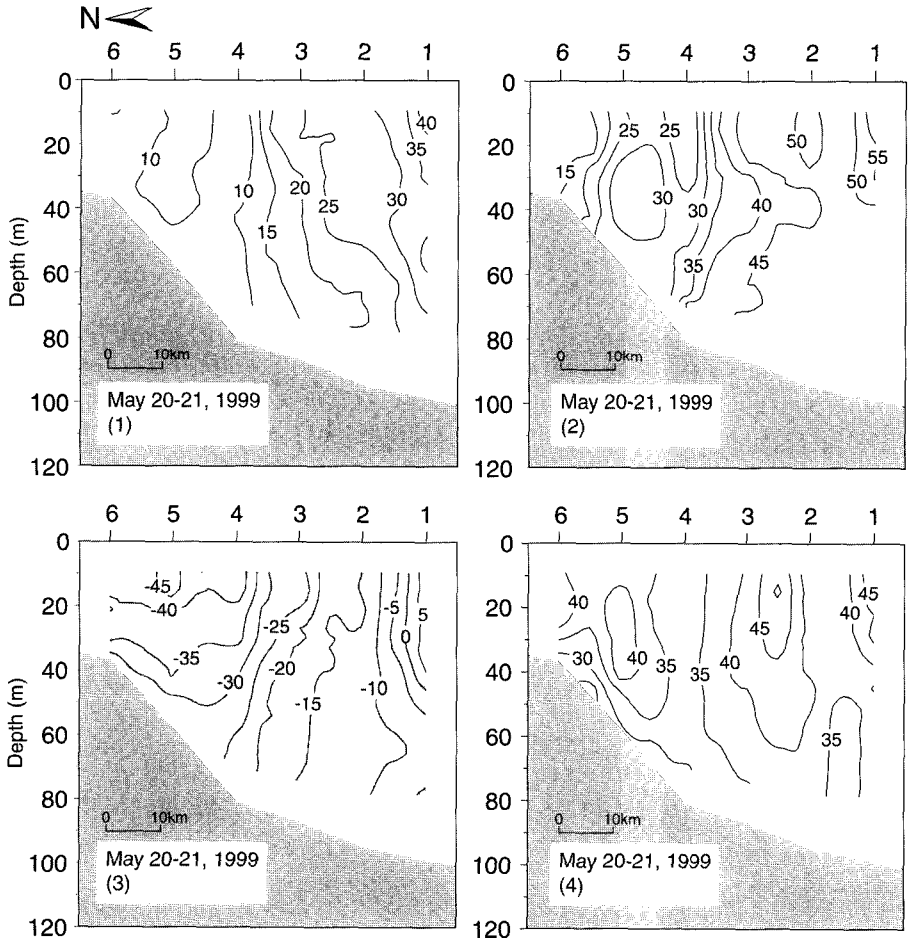

Fig. 5. Cross sections of E-component velocity on individual tracks.

TIME SERIES DATA

Tidal height

Tides in the South Sea are predominantly semidiurnal. The maximum tidal range, as measured between consecutive peak and trough, was 396 cm at Yosu and 364 cm at Site-M, both occurring on 16 May. The result of harmonic analyses of tides (Foreman, 1977) at Yosu and Site-M are compared in Table 1. Only constituents with amplitudes larger than 5 cm are presented. Amplitudes of diurnal constituents are greater at Site-M whereas those of semidiurnal are greater at Yosu, having Form Factors of 0.2 at Yosu and 0.3

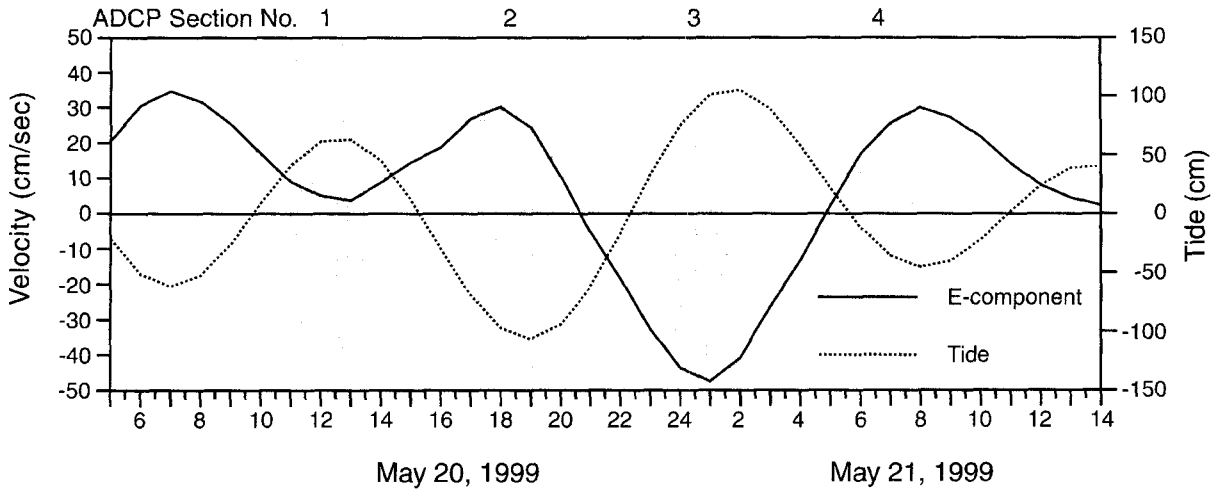

Fig. 6. Tidal current (E-component) and surface height during the May cruise. Shaded regions indicate times of V/M ADCP sections.

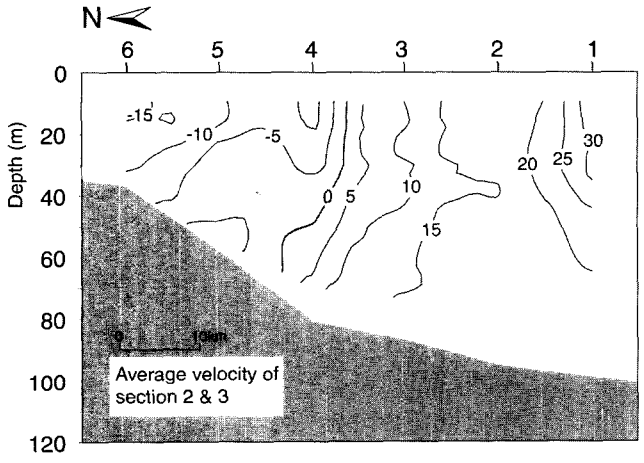

Fig. 7. Vertical distribution of E-velocity after averaging of cross sections 2 and 3 in Fig. 5.

Table 1. Comparison of tides at Yosu and ADCP site (M): Amplitude (cm)/Greenwich phase (°) and phase lag (min) are given

Tide	Period (hrs)	Yosu	Site-M	Lag (min)
O_1	25.82	12.6/20.8	15.2/43.5	97.6
P_1	24.07	5.9/53.0	7.2/73.1	80.6
K_1	23.93	17.9/45.9	21.8/66.0	80.1
μ_2	12.87	6.5/330.8	6.8/336.1	11.4
N_2	12.66	20.0/355.5	18.5/5.1	20.2
M_2	12.42	96.3/359.2	86.6/9.5	21.3
S_2	12.00	43.1/24.9	38.7/33.5	17.2
K_2	11.97	11.7/47.3	10.5/55.9	17.1

at Site-M. Tides at Site-M lag behind those at Yosu by more than 1 hr for diurnal constituents and 17–21 minutes for semidiurnal.

Tidal current

Tidal velocity has been predicted by harmonic analysis (Foreman, 1978) at each depth, then subtracted from the original hourly data to determine nontidal velocity. Subtidal velocity is obtained by applying a Butterworth filter with 40-hour cutoff period to this nontidal velocity to remove higher frequency fluctuations. The subtidal E-component at 10 m depth is demonstrated in Fig. 8. Maximum and minimum velocities are 94.4 cm/s and −77.8 cm/s, respectively. Mean and standard deviation for each case of total, tidal, nontidal and low-passed are 10.3±25.4 cm/s, 0.0±21.2 cm/s, 10.4±13.8 cm/s and 10.2±9.9 cm/s, respectively. It is noted that tidal velocity has a zero mean while other components have an eastward mean velocity of about 10 cm/s. Low-passed velocity has the smallest standard deviation.

Table 2 is the result of harmonic analysis for tidal current at 10 m as an example. Only the components with semi-major axis greater than 3 cm/s are shown in the table. Inclination angle is direction of the semi-major axis measured counterclockwise from east. The sign of the semi-minor axis distinguishes the sense in which the current vector rotates, i.e., positive (negative) value means counterclockwise (clockwise) rotation of the tidal ellipse. Diurnal currents rotate clockwise while the other constituents rotate counterclockwise.

Harmonic constants of the four major constituents of tidal height as a function of depth are given in Fig. 9. M_2 has the largest amplitude, about 22.5 cm/s, followed by K_1, O_1 and S_2. Vertical changes in ampli-

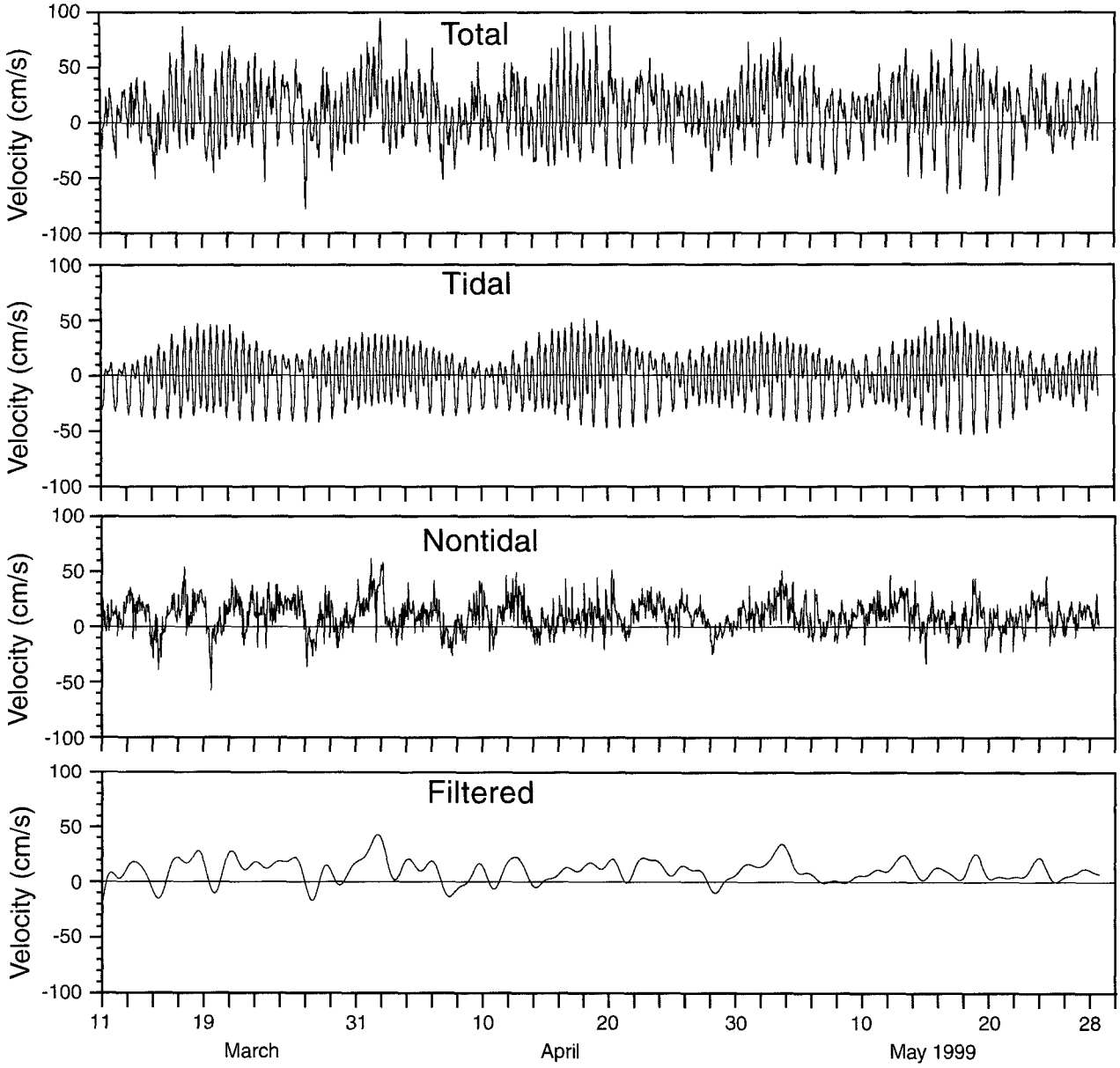

Fig. 8. Time series of total, tidal, nontidal and low-passed velocity (E-component).

Table 2. Tidal current ellipse at 10 m depth

Tide	Period (hrs)	Major (cm/s)	Minor (cm/s)	Inc. angle (°)	Phase (°)
O_1	25.82	11.7	−2.6	18.2	302.9
P_1	24.07	3.6	0.2	20.3	179.8
K_1	23.93	14.6	−23.3	22.5	177.5
N_2	12.66	4.7	0.1	1.7	163.2
M_2	12.42	22.4	1.4	177.3	352.3
S_2	12.00	8.9	1.3	4.8	204.1

tude are small except K_1. There is no significant change in phase with depth. The apparent 180° shift in S_2 at 46 m depth is caused by a change in the choice of reference axis. Tidal current ellipses at selected depths (Fig. 10) show that the diurnal components have greater angles of semi-major axes from the east and rotates in clockwise direction.

Fig. 11 is a result of autospectra for alongshore (U) and offshore (V) components of current in the local coordinate system described in the next section. The alongshore component is generally more than 10 times greater than the offshore one. Diurnal and semidiurnal peaks are very pronounced, with the latter being dominant. As a result, total kinetic energy of tidal current is 3–5 times larger than nontidal current for the alongshore component. For the offshore

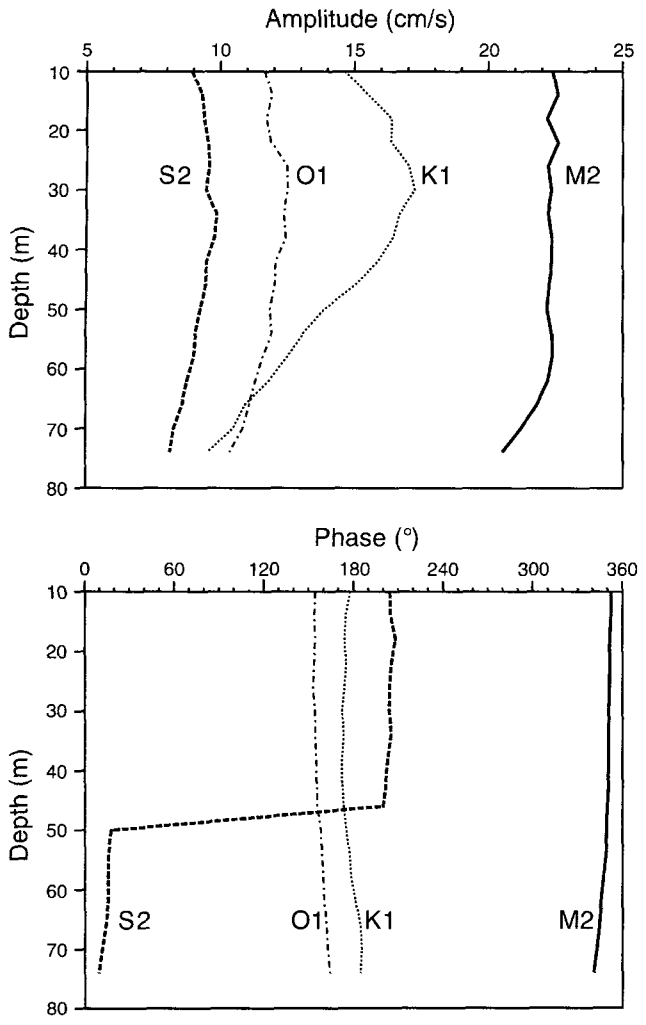

Fig. 9. Amplitude of major axis and Greenwich phase vs. depth for the four strongest tidal components.

component, however, the situation is reversed. Tidal energy is only 40–90% of the nontidal component. Tidal/nontidal ratios for both components increase with depth in common. The weakness of the offshore component means that tidal current is more rectilinear. The broad peak at about 0.01 cph is also significant. This subtidal variability with period of about 4 days is a very characteristic feature as shown in a later section.

Mean current and local coordinate systems

Mean velocity and standard deviation ellipse of the tide-removed data were computed at the original 4 m intervals, but are shown at 8 m intervals in Fig. 12 to avoid the overlapping of ellipses.

Mean speed increases gradually from 10.8 cm/s at 10 m to 14.4 cm/s at 66 m then decreases to 13.1 cm/s at 74 m in the bottom boundary layer. Direction decreases from 15.6° (anticlockwise from east) at 10 m to 11.8° at 26 m then increases again to 23.7° at 66 m and more rapidly to 36.8° at 74 m. Depth-averaged direction and speed excluding the bottom boundary layer is 15° and 12.8 cm/s, respectively. Direction of the semi major axis changes in the same manner as the mean velocity does, except it has low angle of 26° near the bottom. Principal component parallel to the semi major axis contains 82–88% of total variance.

Considering the topography and direction of mean velocity in the upper layer, the local coordinate system is rotated 15° anticlockwise. Both current and wind components parallel to the rotated local x-axis are referred to as U-component or alongshore velocity.

Subtidal variability

The time series data were low-pass filtered using the Butterworth Filter with 40-hour cutoff frequency in order to remove the tidal components. The first vertical EOF mode for the E-component of velocity, representing the barotropic portion of subtidal variability, has 96.2% of the total variance and the second mode 2.5%. Hence, the current is predominantly barotropic in spring. For the N-component, corresponding values for the first and second mode are 86.7% and 6.9%, the reduced values being due to veering in the bottom boundary layer.

The temporal change of subtidal velocity vectors at several depths (Fig. 13) shows that the current was dominantly eastward with occasional reversals. Temporal changes in direction and magnitude occurred in the same fashion at every depth, again indicating that the current is largely barotropic. Before 15 April the current is generally weak and variable. Currents alternate between clockwise and counterclockwise rotation 8 times, probably due to the shifting of the front and meander motion. As noticed in the hydrographic section (Fig. 2), Site-M is close to the front so that current observed there will be sensitive to changes in frontal position. Eastward current is more persistent after mid-April, with strongest currents in the layers from 42 m to 62 m. Note that the current is especially weak in the upper layer of 10–30 m depth after 15 May. Current variability is more visually comprehensive in Fig. 14. Baroclinicity increases to some extent in May. Current direction reversed 23 times during the whole period, which yields the average interval of about 4 days.

In addition to the dominant influence of the TWC,

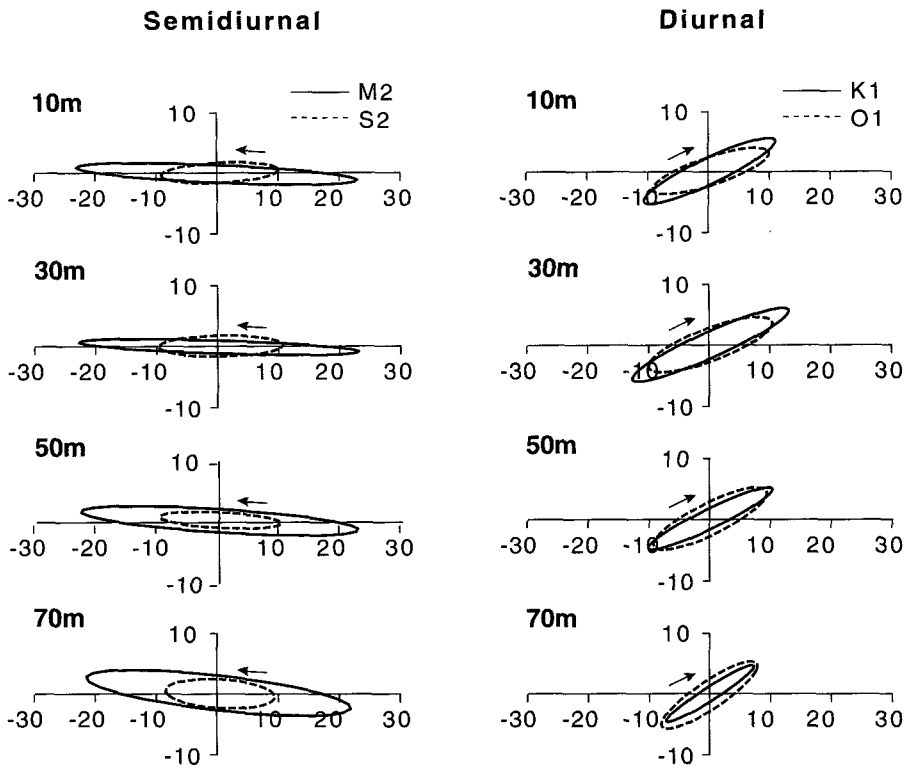

Fig. 10. Tidal current ellipses at representative depths.

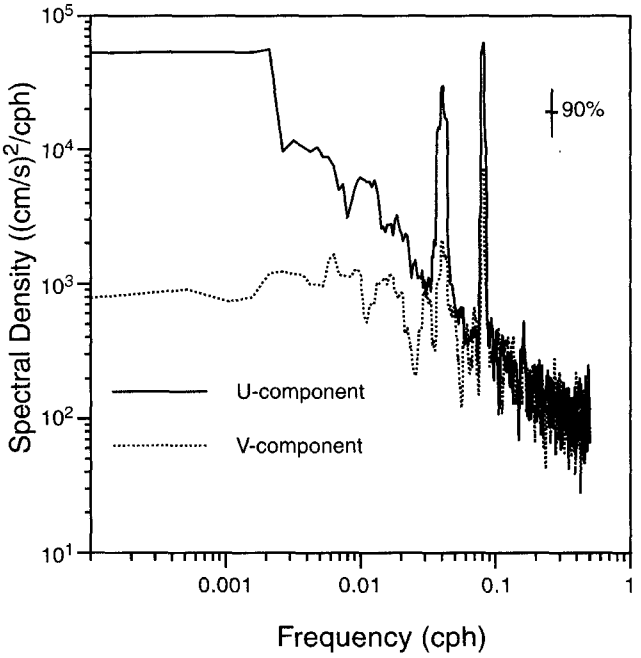

Fig. 11. Autospectra of current velocity at 10 m depth.

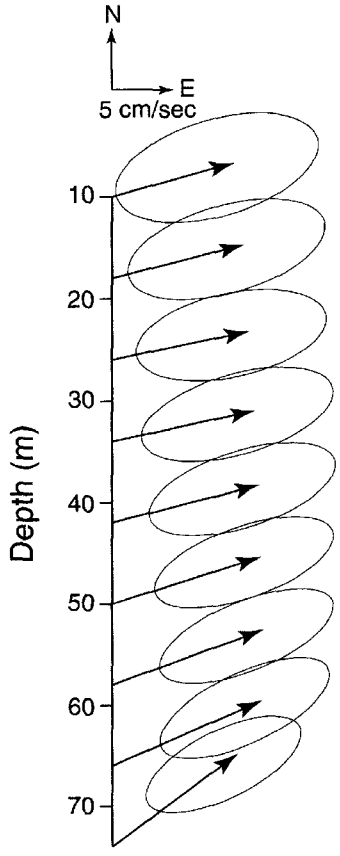

Fig. 12. Vertical distribution of mean current vectors and standard deviation ellipses at Site-M.

circulation in the South Sea may be affected by wind. In order to investigate the causal relationship, Fig. 15 compares the time series of alongshore wind at Yosu, sea level at Site-M, alongshore current (U) at 10 m, offshore current (V) and sea level difference (Site-M Yosu). Sea level variations at both sites are

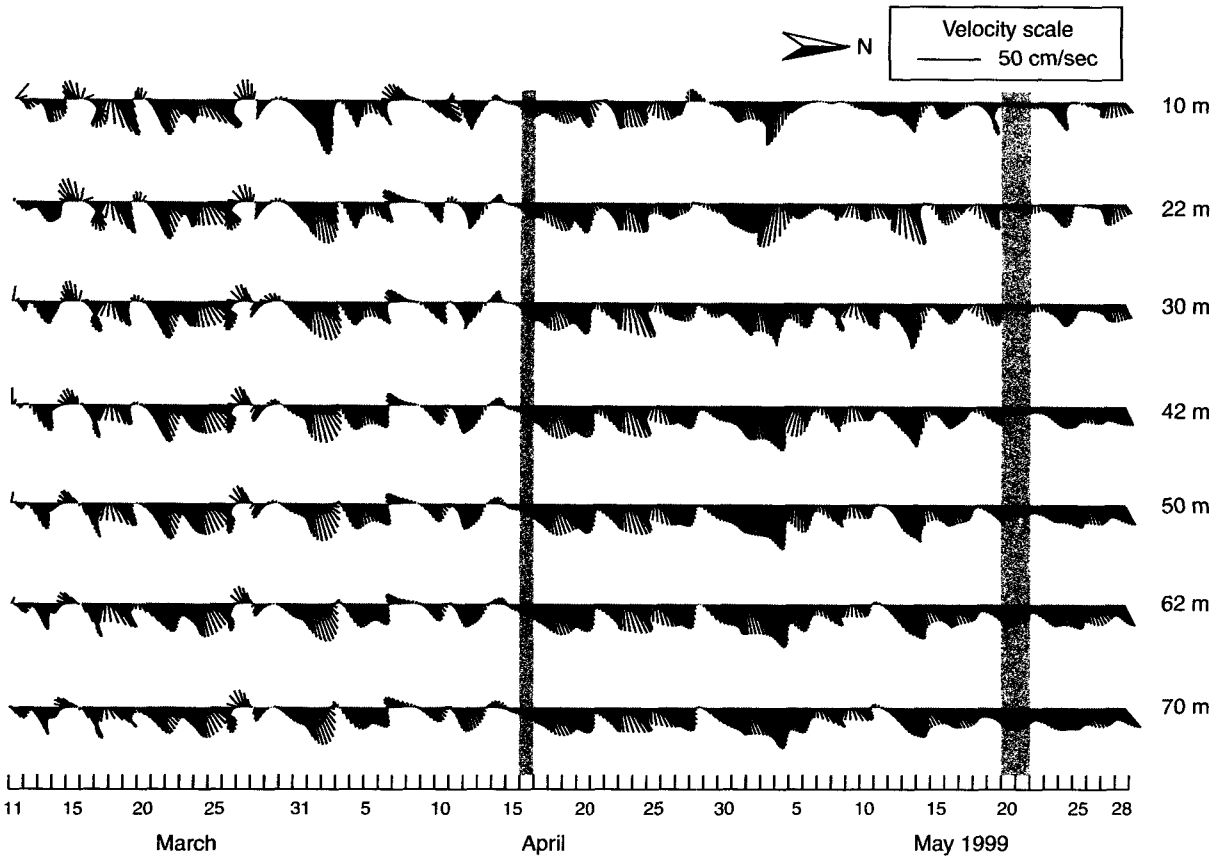

Fig. 13. Stick vector plot of low-passed velocity for various depths. Vertical shaded bars are the periods of CTD observations.

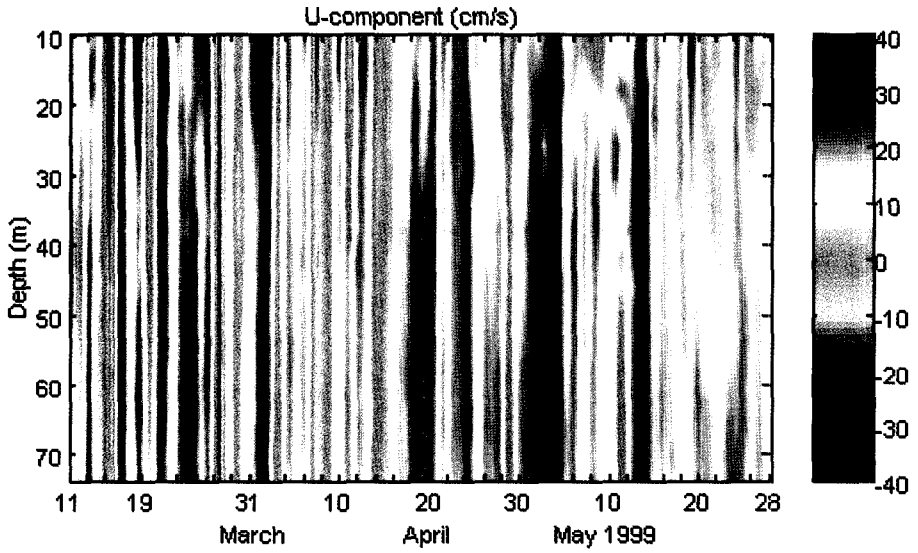

Fig. 14. U-component of velocity vs. time and depth at Site-M.

nearly the same (not shown) and have some mirror image against the alongshore wind. Sea level drops with the increase in eastward (positive) wind and *vice versa* (Fig. 15a). This inverse correlation is confirmed in the frequency domain (Fig. 16a). Coherence of wind and sea level is significant at all frequencies. A peak at about 80-hour period (0.012 cph) is most pronounced and corresponds to a phase difference of almost 180°. We interpret this connection as the result of Ekman-like dynamics; a positive wind leads to an offshore current and a resulting set-down of the sea surface.

If the wind effect is significant, changes in along-

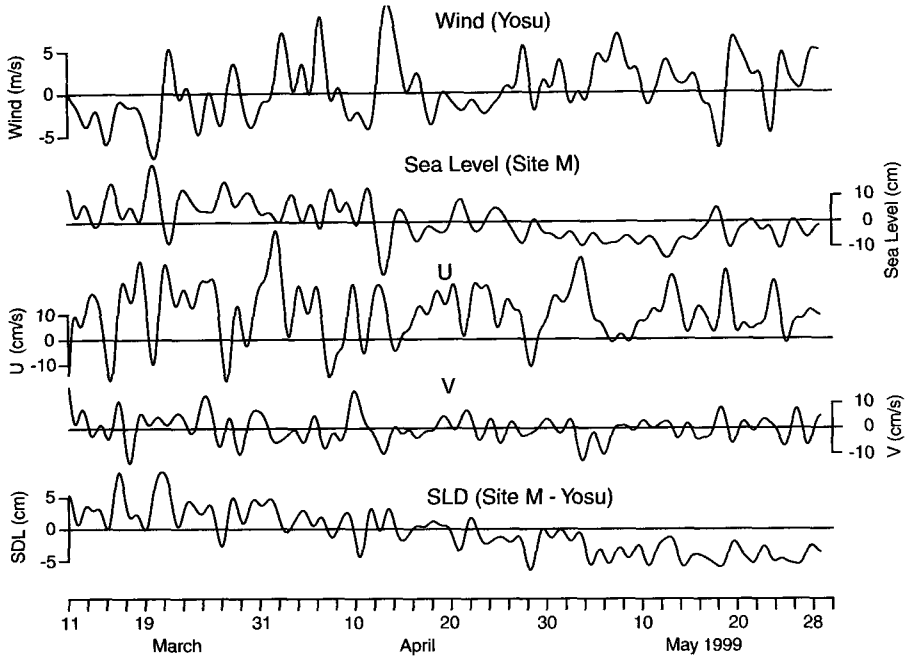

Fig. 15. Time series of along-shore wind, current, sea level, and sea level difference.

shore wind should lead the variations of offshore current. When the geostrophic influence is effective, the sea level slope induced by any offshore current will develop an alongshore current. In the time series (Fig. 15) however, it is not easy to find the clear wind-current relations. In the frequency domain (Fig. 16b), the offshore current is coherent with wind at 0.006 cph (about 7-day period) with phase of almost 180°. This means that eastward (positive) wind leads the offshore (negative) current. Alongshore current is significant at 0.012 cph (about 4-day period). The phase relation should be interpreted that the wind leads the current with large phase lag.

For the current-sea level relations, the alongshore current shows a good inverse correlation especially in the first half of the series in the time series of Fig. 15. Sea level drops are related with increased current. There are many occasions when the peaks in velocity curve slightly lead the troughs in sea level. This relation is also identified from the coherence analysis (Fig. 16c). There is a major significant peak at 0.011 cph with a phase lag of about 180°. The offshore current is coherent at similar frequency bands but the coherence is low.

Sea level difference is compared with alongshore current (Fig. 16d). If the current is observed between two tide gauges and geostrophy is satisfied, there would be a good linear relationship between SLD and current. In this case, however, the offshore data of sea level is only available at the same ADCP site. In spite of this unfavorable condition, SLD-current relation is tested by the available data. There is no visual consistency in variations of both time series. For only a few instances SLD increase leads the strengthening of the current. Nevertheless, in the frequency domain (Fig. 16d), two peaks are significant at about 10-day and 80-hour periods. Both have a stable phase of about −60°; that is, SLD leads the alongshore current by that amount.

For all cases considered, a common feature is the significant coherence at about 4-day period. The same periodicity of coherence is also found in the southeast coast (Lee *et al.*, 2003). Lyu *et al.* (2002) explained that this periodicity is due to the atmospheric pressure variation over the East Sea that affects the transport through the Korea Strait.

SUMMARY AND CONCLUSIONS

A TRBM with ADCP and tide gauge was deployed near the South Sea Front in spring 1999 off the central south coast of Korea at 80 m depth. CTD observation as well as V/M ADCP profiling were repeated at six-hour interval to obtain the tide-removed velocity field. The waters are homogeneous in early spring. With the developing stratification in late spring, isotherms form that deepen with increasing water depth south of the front, whereas the isohalines there are of retrograde type. The result of this T–S distribution is a region of shallow isopycnals, which we identify as the frontal position, with isopycnals deepening to either side. Using the V/M ADCP and bottom-mounted

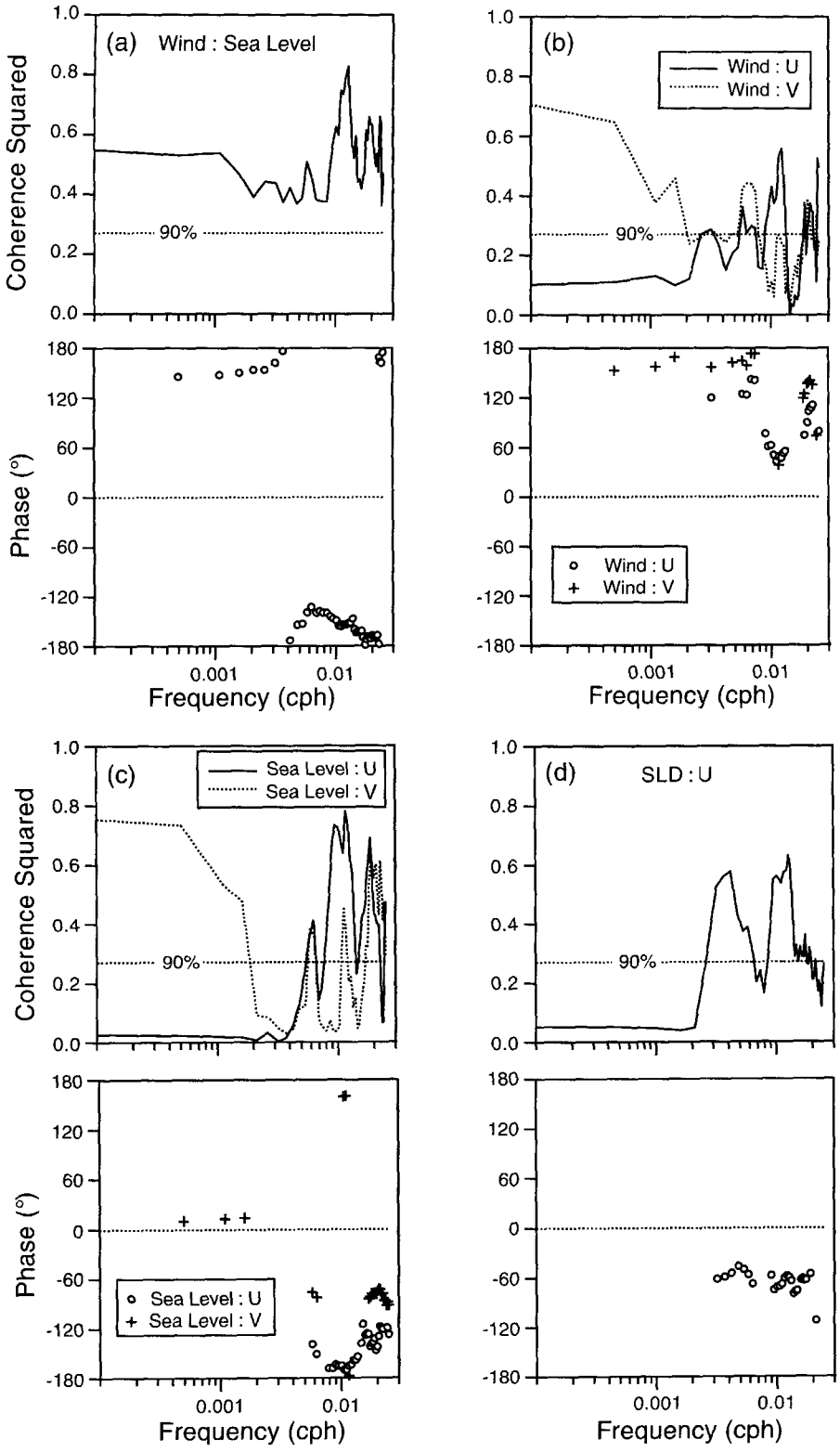

Fig. 16. Coherence spectra for the indicated pairs of variables.

ADCP and tide gauge measurements together, it has been shown that currents in the coastal region north of the front are westward and those to the south are eastward.

The structure of current is essentially barotropic in spring although baroclinicity increases to some degree in May. Kinetic energy of the tidal current is 3–5 times larger than that of the nontidal current. The low-frequency current shows either alternating clockwise and counterclockwise rotation or else persistent

eastward velocity, depending on the frontal motion. Wind, sea level and current are coherent at period of about 4 days. Alongshore winds at Yosu and subtidal variability of sea surface height are consistent with Ekman-like dynamics.

ACKNOWLEDGEMENTS

This study is a part of the research project of the Korea Inter-university Institute of Ocean Science at Pukyong National University supported by the Korea Research Foundation in 1999. We appreciate the untiring help of the crew of R/V *Tamyang* in deploying ADCP/TRBM and hydrographic observations.

REFERENCES

Chang, K.-I., M.-S. Suk, I.-C. Pang and W. J. Teague, 2000. Observations of the Cheju Current. *J. Korean Soc. Oceanogr.*, **35**: 129–152.

Foreman, M.G.G., 1977. Manual for tidal heights analysis and prediction. Pacific Marine Science Report 77-10, Institute of Ocean Sciences, Patricia Bay, Victoria, B.C., 101 pp.

Foreman, M.G.G., 1978. Manual for tidal currents analysis and prediction. Pacific Marine Science Report 78-6, Institute of Ocean Sciences, Patricia Bay, Victoria, B.C., 69 pp.

Hsueh, Y., 1988. Recent current observations in the eastern Yellow Sea. *J. Geophys. Res.*, **93**: 6875–6884.

Lee, J.C., 1983. Characteristics of front near the Cheju Strait in early winter. *Bull. Korean Fish. Soc.*, **16**: 51–58.

Lee, J.C., J.Y. Na and S.-D. Chang, 1984. Thermohaline structure of the shelf front in the Korea Strait in early winter. *J. Oceanol. Soc. Korea*, **19**: 56–67.

Lee, J.C., S.-R. Lee, S.-K. Byun, M.-J. Park, J.-C. Kim and H.-J. Yoon, 1998. Variability of current and sea level difference in the western channel of the Korea Strait in winter 1995-96. *J. Fish. Sci. Tech.*, **1**: 276–282.

Lee, J.C., D.H. Kim and J.-C. Kim, 2003. Observations of upwelling at Ulsan in summer 1997. *J. Korean Soc. Oceanogr.*, **38**: 122-134.

Lyu, S.J., K. Kim and H.T. Perkins, 2002. Atmospheric pressure-forced subinertial variations in the transport through the Korea Strait. Geophys. Res. Lett., 29: 10.1029/2001GL014366.

Ro, Y.J., M.-J. Park, S.-R. Lee and Lee, J.C., 1995. Structure and variability of the T-S field and the current across the Korea Strait. J. Korean Soc. Oceanogr., **30**: 237–249.

Shim, T.B., W.J. Wiseman Jr., O.K. Huh and W.-S. Chuang, 1984. A test of the geostrophic approximation in the western channel of the Korea Strait. In: Ichiye, T. (Ed.), *Ocean Hydrodynamics of the Japan and East China Seas*, Elsevier Science Publishers B. V., Amsterdam, pp. 263–272.

Teague, W.J., H.T. Perkins, Z.R. Hallock and G.A. Jacobs, 1998. Current and tide observations in the southern Yellow Sea. *J. Geophys. Res.*, **103**: 27783–27793.

Manuscript received August 4, 2003
Revision accepted September 26, 2003
Editorial handling: Jae-Hak Lee